INORGANIC CHEMISTRY
FRONTIERS

RESEARCH ARTICLE

View Article Online
View Journal | View Issue

Cite this: *Inorg. Chem. Front.*, 2022, **9**, 2880

Structural investigation of the efficient capture of Cs^+ and Sr^{2+} by a microporous Cd–Sn–Se ion exchanger constructed from mono-lacunary supertetrahedral clusters†

Jia-Ying Zhu,‡[a] Lin Cheng, ‡[b] Yi-Ming Zhao,[a] Meng-Yu Li,[a] Zi-Zhao Wang,[a] Juan Wang,[a] Cheng Wang [a] and Kai-Yao Wang *[a]

Visualization of the ion exchange mechanism for ^{137}Cs and ^{90}Sr decontamination is important for safe radioactive liquid waste reprocessing and emergency response improvement in the event of a nuclear accident. Here, the remediation of Cs^+ and Sr^{2+} was achieved through ion exchange using a cadmium selenidostannate, $[CH_3NH_3]_3[NH_4]_3Cd_4Sn_3Se_{13}\cdot 3H_2O$ (**CdSnSe-1**), with rapid exchange kinetics, high β/γ radiation resistances, broad pH durability and facile elution. The framework constructed from mono-lacunary supertetrahedral clusters features a great negative charge density of 3.27×10^{-3} that accounts for the superhigh exchange capacities of 371.4 (Cs^+) and 128.4 mg g^{-1} (Sr^{2+}). Single-crystal structural analysis on the exchanger during the "pristine–ion exchange–elution" cycle supplies instructive information to elucidate the uptake and recycle mechanism for Cs^+ and Sr^{2+}. The broken symmetry of the cluster caused by a vacant site, combined with the co-templating effects of mixed methylammonium/ammonium, contributes to the formation of voids I and II that show adsorption activity for both Cs^+ and K^+ ions. In comparison, the divalent Sr^{2+} ions with higher hydration degree exchange with (alkyl) ammonium cations in a 1 : 2 molar ratio, resulting in its location at a new void (III) closer to the framework and thus a higher binding strength. The energy variation during the adsorption process based on a DFT calculation illustrates the high efficiency of **CdSnSe-1** for capture of both Cs^+ and Sr^{2+}. This "visualized" ion exchange underlines the robustness and flexibility of **CdSnSe-1** as a Cs^+ and Sr^{2+} trapper, and reveals the deeper structure–function relationship from a new surface interaction viewpoint.

Received 14th February 2022,
Accepted 15th April 2022

DOI: 10.1039/d2qi00338d

rsc.li/frontiers-inorganic

Introduction

The rapid growth of the nuclear energy industry has brought about an increasing amount of hazardous radionuclides that can cause significant damage to the environment and public health.[1,2] ^{137}Cs and ^{90}Sr, with half lives of around 30 years, are two primary fission products from ^{235}U, and they can emit β or γ radiation and exhibit high levels of toxicity for human bodies, especially for people affected by nuclear accidents.[3,4] For example, the Fukushima nuclear leakage accident in 2011 resulted in the release of large quantities of $^{137}Cs^+$ and $^{90}Sr^{2+}$ ions into the surrounding environment. With a high migration ability, they are enriched in water,[5] soil,[6] forest vegetation[7] and other organisms.[8] Upon ingestion, $^{137}Cs^+$ can accumulate in body fluid/soft tissues and cause damage or death to cells,[9] while $^{90}Sr^{2+}$ is preferentially fixed in bone mass and increases the risk of illnesses like osteoporosis, leukemia, or even bone cancer.[10,11] On the other hand, $^{137}Cs^+$ and $^{90}Sr^{2+}$ ions generate large amounts of heat during their decay processes, which pose a requirement for greater storage room and better encapsulation technology in geological repositories.[12] This leads to a great risk for the storage of nuclear liquid waste over a long period. In this context, the efficient removal of $^{137}Cs^+$ and $^{90}Sr^{2+}$ can not only improve the emergency response capability in the event of a nuclear accident, but also reduce the cost and burden of safer nuclear liquid waste reprocessing. The recovered ^{137}Cs and ^{90}Sr radionuclides can be further purified as excellent heating or radiation sources for nuclear batteries,

[a]*Tianjin Key Laboratory of Advanced Functional Porous Materials, Institute for New Energy Materials and Low-Carbon Technologies, School of Materials Science and Engineering, Tianjin University of Technology, Tianjin 300384, P.R. China. E-mail: kaiyao0729@163.com*
[b]*College of Chemistry, Tianjin Normal University, Tianjin 300387, P. R. China*

†Electronic supplementary information (ESI) available: Powder XRD patterns, FTIR, EDS, mapping, UV–vis reflectance spectra and TG analysis on the pristine, exchanged and eluted products. CCDC 2133519–2133523 (for **CdSnSe-1**, **CdSnSe-1Cs**, **CdSnSe-1Sr**, **CdSnSe-1Cs-K** and **CdSnSe-1Sr-K**). For the ESI and crystallographic data in CIF or another electronic format see DOI: **https://doi.org/10.1039/d2qi00338d**

‡These authors contributed equally to this work.

thermoelectric generators and cancer radiotherapy, providing feasible ways for their recycling and comprehensive utilization.[13–15]

Hitherto, Cs^+ and Sr^{2+} pollutants have been eliminated through a variety of technologies, like precipitation,[16,17] solvent extraction,[18,19] membrane filtration,[20,21] biological treatment,[22,23] and ion exchange.[24,25] However, there are some specific disadvantages with these methods. For example, precipitation cannot sufficiently reduce the ion concentration below the limit level to meet the relevant water quality standards, and moreover, it introduces large quantities of salt ions or solution pH deviation, which necessitates complex secondary treatment. The application of solvent extraction is subject to the use of toxic organic extractants. Membrane filtration suffers from membrane fouling, low recovery rate and high energy consumption. Moreover, biological treatment is usually sensitive to pH, temperature, nutrient availability, *etc*. and thus the microbes could be readily inhibited or poisoned as they encounter a sudden change of environment. In comparison, ion exchange emerges as a promising method for Cs^+ and Sr^{2+} removal owing to its high efficiency, facile operation, and simple device, to name several advantages. In most cases, the ion exchange method will produce high-quality treated effluent, and it will not cause secondary pollution due to the safe landfill disposal of used adsorbents. Inorganic porous materials with high radiation and thermal stabilities have been extensively employed for the removal of radioactive Cs^+ and Sr^{2+}, as confirmed by the great development made in research on zeolites,[26,27] clays,[28,29] titanium silicates,[30,31] phosphates,[32,33] molybdates,[34] *etc*. However, these oxide exchangers usually lose their activities in acidic/alkaline or highly salty environments, and thus cannot be used in the extreme conditions in the practical treatment of nuclear liquid wastes. Therefore, developing new advanced materials for the effective removal of Cs^+ and Sr^{2+} from aqueous solutions has recently received extensive public attention.

Metal chalcogenide materials with labile extra framework cations are a type of prospective ion exchanger because they possess soft chalcogen atoms (*e.g.* S, Se) that show a strong affinity to softer metal cations against harder H^+, Na^+ or Ca^{2+}. Hitherto, important progress has been obtained on the uptake of Cs^+ and Sr^{2+} by metal sulfides, *e.g.* KMS-1,[35] KMS-2,[36] KTS-3,[37] FJSM-SnS,[38] ZnSnS-1,[39] InS-1,[40] InS-2,[41] KZTS,[42] NaTS,[43] SbS-1K,[44] oxysulfides as InSnOS materials,[45,46] and selenides like $K_{14}Cd_{15}Sn_{12}Se_{46}$,[47] CuGeSe-1,[48] and AgSnSe-1.[49] These ion exchangers exhibit fast exchange kinetics, superior capacities, excellent selectivity and good acid/base and radiation resistances. However, there are still serious unresolved issues that hinder the design and preparation of new advanced exchangers. One of the issues is the uncertainty of the exact adsorption site for Cs^+ and Sr^{2+} in most cases due to the lack of good crystallinity on the exchange process, as limited to recent examples including InSnS-1,[50] FJSM-SbS,[51] ZnSnS-1,[39] CuGeSe-1,[48] and AgSnSe-1.[49] In addition, the effects of the chemical environment on adsorption selectivity are not well understood, especially for cases where the intercalation of larger hydrated ions is inhibited to some extent. This context proposes higher requests for the study of the ion exchange mechanism at a molecular level, which relies on the building of a robust chalcogenide framework with versatile tunnels/voids for cation encapsulation.

Highlighted here is a porous material construction strategy using lacunary supertetrahedral clusters as building units, which is proposed primarily for the following three reasons. (a) With large size and remarkable interlinking capability, the supertetrahedral clusters prove to be effective building units for constructing microporous frameworks with an open tunnel system, which is a critical premise for the transfer of metal ions. (b) The formation of vacant sites in the cluster would cause molecular symmetry breaking and thus enrich the specific voids (*i.e.* adsorption sites) with different chemical environments to detect their distinction in metal uptake. (c) As illustrated previously,[40] the employment of lacunary clusters as building units can effectively increase the negative charge density of the framework, which is beneficial for elevating the theoretical exchange capacity of ion exchangers. In the present work, this hypothesis was achieved by the deep eutectic solvothermal preparation of a cadmium selenidostannate, namely $[CH_3NH_3]_3[NH_4]_3Cd_4Sn_3Se_{13}\cdot 3H_2O$ (**CdSnSe-1**), which is constructed from the interlinkage of mono-lacunary P1-$[Cd_4Sn_3Se_{16}]^{12-}$ clusters. **CdSnSe-1** exhibits high ion exchange capacities for both Cs^+ (371.4 mg g^{-1}) and Sr^{2+} (128.4 mg g^{-1}), together with rapid kinetics, wide pH durability, high radiation resistance, facile elution and good selectivity against various alkali/alkaline earth metal cations. Impressively, the structural distinction of adsorption sites caused by cluster symmetry breaking and its effect on the adsorption selectivity for Cs^+ and Sr^{2+} was first revealed on the basis of the successful collection of single-crystal structures for pristine, Cs^+ and Sr^{2+} exchanged (**CdSnSe-1Cs** and **CdSnSe-1Sr**) and K^+ elution products (**CdSnSe-1Cs-K** and **CdSnSe-1Sr-K**). This work visualizes the intercalation and elution of Cs^+ and Sr^{2+} at the molecular level, not only opening up a new perspective clarifying the ion exchange mechanism, but also underlining the metal chalcogenides constructed from lacunary clusters as advanced ion exchangers for radionuclide decontamination (Fig. 1).

Experimental section

Materials

$CdCl_2\cdot 2.5H_2O$ (99%, Sinopharm Chemical Reagent Co. Ltd), Sn (99.99% Aladdin Reagent Co. Ltd), Se (99.99%, Aladdin Reagent Co. Ltd), diethylamine hydrochloride (99%, Aladdin Reagent Co. Ltd), *N*,*N*′-dimethylurea (98%, Aladdin Reagent Co. Ltd), hydrazine hydrate (>98%, Aladdin Reagent Co. Ltd), CsCl (99.9%, Aladdin Reagent Co. Ltd), $SrCl_2\cdot 6H_2O$ (99.5%, Shanghai Macklin Biochemical Co. Ltd), NaCl (GR, Sinopharm Chemical Reagent Co. Ltd), KCl (GR, Aladdin Reagent Co. Ltd), $MgCl_2\cdot 6H_2O$ (99%, Shanghai Macklin Biochemical Co. Ltd), $CaCl_2\cdot 2H_2O$ (98%, Beijing J&K Scientific Co. Ltd), hydrochloric acid (AR, Sinopharm Chemical Reagent Co. Ltd) and NaOH

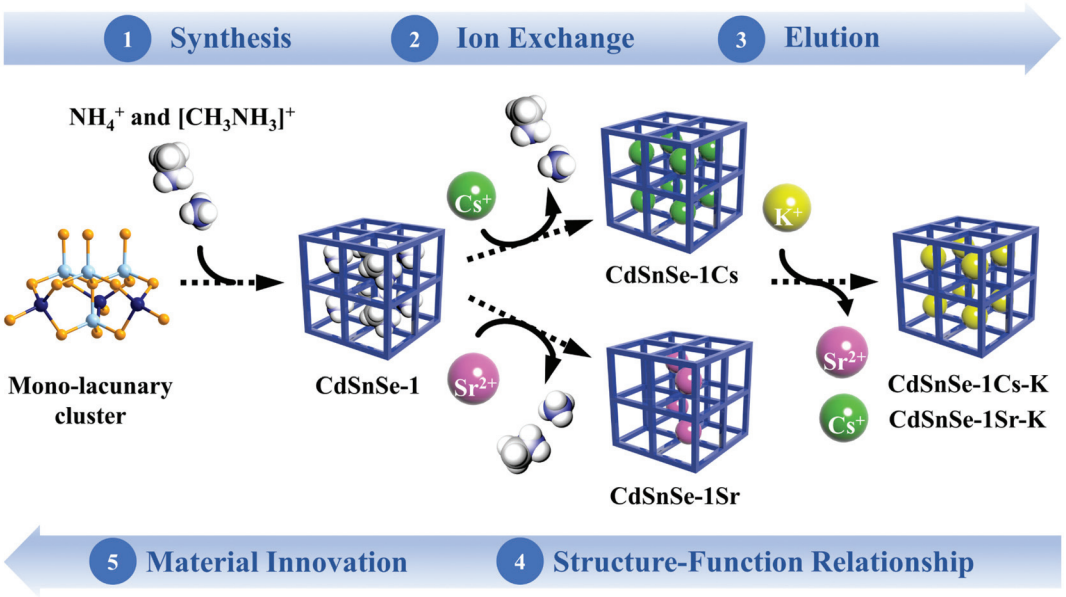

Fig. 1 Schematic representation for the construction of **CdSnSe-1** and the following Cs^+, Sr^{2+} ion exchange and K^+-elution processes, during which a significant structure–function relationship was revealed for optimizing the design and synthesis of materials.

(AR, Sinopharm Chemical Reagent Co. Ltd) were commercially available reagents and used without additional purification.

Characterizations and irradiation studies

Energy-dispersive spectroscopy (EDS) and elemental distribution maps were recorded on an FEI Quanta FEG 250 scanning electron microscope. FTIR spectra were obtained on a PerkinElmer Frontier Mid-IR FTIR spectrometer using KBr pellets. UV–vis reflectance of the solid-state samples ($BaSO_4$ for 100% reflectance) was recorded on a PerkinElmer Lambda 750 UV–vis spectrophotometer. The absorption spectra were transformed from reflectance spectra according to the Kubelka–Munk function: $F(R) = (1 - R)^2/2R$, where $F(R)$ and R represent the absorption and reflectance, respectively.[52] Powder X-ray diffraction (XRD, Cu-Kα, λ = 1.54178 Å) was performed on a Rigaku SmartLab 9 kW diffractometer. X-ray photoelectron spectroscopy (XPS) was performed on a Thermo Scientific ESCALAB 250Xi spectrometer. H, C, and N elemental analyses of solid-state samples were performed using an Elementar Vario EL cube instrument. ^1H and ^{13}C NMR of the samples was performed on a Bruker Avance III 400 instrument at room temperature, and mixed $N_2H_4{\cdot}H_2O$ (98%)/D_2O was used as the solvent. The metal ion concentrations were measured using a Vista-MPX Varian inductively coupled plasma optical emission spectrometer (ICP-OES) and a ThermoFisher iCAP RQ inductively coupled plasma mass spectrometer (ICP-MS). **CdSnSe-1** single crystals were irradiated using γ ray for 100 kGy (1.2 kGy h^{-1}) and β ray for 100 and 200 kGy (50 kGy h^{-1}). The γ irradiation was conducted using a ^{60}Co source that was provided by Suzhou CNNC Huadong Radiation Co. Ltd, Jiangsu Province, China. The β irradiation was performed using 10 MeV electron beams that were generated using an electron accelerator from CGN Dasheng Electron Accelerator Co. Ltd., Jiangsu Province, China.

Synthesis of CdSnSe-1

A mixture of $CdCl_2{\cdot}2.5H_2O$ (0.305 g, 1.33 mmol), Sn (0.119 g, 1 mmol), Se (0.42 g, 5.32 mmol), diethylamine hydrochloride (0.384 g, 3.5 mmol), *N*,*N*′-dimethylurea (0.617 g, 7 mmol) and $N_2H_4{\cdot}H_2O$ (0.8 mL, 16.5 mmol) was sealed in a 25 mL Teflon liner encapsulated in a stainless steel reactor and heated at 160 °C for 3 days. After natural cooling to room temperature, the product was washed using deionized water and then dried in air. Pure orange block-like crystals of **CdSnSe-1** were collected in a mass of 0.48 g, with a yield of 70.7% based on Sn. Anal. calcd for $C_3H_{36}N_6O_3Cd_4Sn_3Se_{13}$ (**CdSnSe-1**, FM = 2036.53): C, 1.769; H, 1.782; N, 4.127. Found: C, 1.791; H, 1.980; N, 4.151.

Ion exchange experiments

Ion exchange experiments were conducted using nonradioactive Cs and Sr isotopes in a typical batch method at a *V*/*m* ratio of 1000 mL g^{-1}. A quantity of 20 mg of **CdSnSe-1** was added to a covered vial containing 20 mL of CsCl or $SrCl_2$ aqueous solution with predetermined Cs^+ or Sr^{2+} concentrations, and the mixture was constantly stirred at room temperature (~20 °C) for 24 h to reach the adsorption equilibrium. Thereafter, the exchanged product was collected by filtration (Whatman 102 paper) and washed using deionized water (DW) and then dried in air. It was characterized using powder XRD, XPS, FTIR, UV–vis, EDS, elemental distribution maps, *etc*. The exchange-saturated products were obtained from 0.1 M CsCl and 0.1 M $SrCl_2$ solutions, and their formulas were defined as $Cs_{5.6}[CH_3NH_3]_{0.2}[NH_4]_{0.2}Cd_4Sn_3Se_{13}{\cdot}3.5H_2O$ (**CdSnSe-1Cs**) and

$Sr_{2.85}[CH_3NH_3]_{0.15}[NH_4]_{0.15}Cd_4Sn_3Se_{13}\cdot 6.5H_2O$ (**CdSnSe-1Sr**), respectively. Anal. calcd for $C_{0.2}H_9Cd_4Cs_{5.6}N_{0.4}O_{3.5}Se_{13}Sn_3$ (**CdSnSe-1Cs**, FM = 2649.52): N, 0.212. Found: N, 0.096. Anal. calcd for $C_{0.15}H_{14.5}Cd_4N_{0.3}O_{6.5}Se_{13}Sn_3Sr_{2.85}$ (**CdSnSe-1Sr**, FM = 2206.49): N, 0.190. Found: N, 0.182. The Cs^+ and Sr^{2+} metal ions in the filtrate need to be diluted to a concentration range below 200 ppb for ICP-MS characterization.

The individual Cs^+ and Sr^{2+} (~6 ppm) ion exchange kinetics were studied in a contact time range of 0–2880 min. The removal rate R (%), distribution coefficient K_d (mL g^{-1}) and equilibrium adsorption amount q_e (mg g^{-1}) were calculated using eqn (1)–(3),

$$R = \frac{C_0 - C_f}{C_0} \times 100\% \quad (1)$$

$$K_d = \frac{V}{m}\frac{(C_0 - C_f)}{C_f} \quad (2)$$

$$q_e = \frac{V}{m}(C_0 - C_e) \quad (3)$$

where C_0 (ppm), C_f (ppm) and C_e (ppm) represent the initial, final and equilibrium concentrations of Cs^+ and Sr^{2+} in aqueous solution, m (g) is the mass of the ion exchanger, and V (mL) is the volume of the test solution. The fitting of the experimental data was conducted using a pseudo-second-order kinetic model as described by eqn (4),

$$\frac{t}{q_t} = \frac{1}{k_2 {q_e}^2} + \frac{t}{q_e} \quad (4)$$

where k_2 (g mg^{-1} min^{-1}) and q_t (mg g^{-1}) represent the rate constant and exchange capacity at time t (min), respectively.

The individual Cs^+ (~3–824 ppm) and Sr^{2+} (~3–741 ppm) ion exchange isotherms were recorded at room temperature for a 24 h contact time. The equilibrium curves were fitted by Langmuir (eqn (5)) and Langmuir–Freundlich (eqn (6)) isotherm models,

$$q_e = q_m \frac{bC_e}{1 + bC_e} \quad (5)$$

$$q_e = q_m \frac{(bC_e)^{1/n}}{1 + (bC_e)^{1/n}} \quad (6)$$

where b (L mg^{-1}) and q_m (mg g^{-1}) account for the Langmuir constant and maximum exchange capacity, respectively, and n is a parameter reflecting the heterogeneity of the system.

The pH effects on the individual Sr^{2+} and Cs^+ (~6 ppm) ion exchange were studied in solutions with the required pH (0–14) that were prepared by diluting Cs^+ or Sr^{2+} from 600 ppm to ~6 ppm using accurately concentrated HCl and NaOH. The contact time for ion exchange was 24 h, and the final pH after the experiment was also measured. The solid product after the ion exchange experiments was checked using powder XRD.

By analogy, the effects of Na^+, K^+, Mg^{2+}, Ca^{2+} cations (0–100 mmol L^{-1}) on the individual Cs^+ and Sr^{2+} (~6 ppm) ion exchange were studied using a similar method, just replacing the pH adjustment with the dissolution of the required amount of NaCl, KCl, $MgCl_2$, $CaCl_2$ in the solution. In addition, deionized water (DW), mineral water (MW, from Nongfu spring), tap water (TW, Xiqing District, Tianjin), and lake water (LW, Tianjin University of Technology, Tianjin) were taken as exchange media to assess the adsorption of Cs^+ or Sr^{2+} in actual environments.

For elution, the Cs^+ and Sr^{2+} exchange-saturated products, *i.e.*, **CdSnSe-1Cs** and **CdSnSe-1Sr** (20 mg for each), were treated with 1 M KCl solution (20 mL) with constant stirring for a contact time of 24 h. The solid products were separated using filtration (Whatman 102 paper), washed and dried in air. The products were characterized using powder XRD, TG, EDS and elemental mapping, and finally defined by the formulas $K_6Cd_4Sn_3Se_{13}\cdot 5H_2O$ (**CdSnSe-1Cs-K**) and $K_{5.3}Sr_{0.35}Cd_4Sn_3Se_{13}\cdot 6.5H_2O$ (**CdSnSe-1Sr-K**).

Crystallography

The indexing and data collection of **CdSnSe-1**, **CdSnSe-1Cs**, **CdSnSe-1Sr**, **CdSnSe-1Cs-K** and **CdSnSe-1Sr-K** single crystals were conducted at 293 K using a Rigaku XtaLab PRO diffractometer with graphite-monochromated Cu Kα radiation (λ = 1.54178 Å). A multi-scan technique was adopted for the absorption corrections. The Cd, Sn and Se atoms in the structure were solved using a direct method (SHELXS-97), and the remaining atoms were revealed by successive Fourier syntheses (SHELXL2014).[53] Refinements were performed for all data using full matrix least squares against $|F|^2$. All of the Cd, Sn, Se, Cs, Sr, K, O, C and N atoms were anisotropically refined, while the hydrogen atoms around the O, C and N atoms were generated with idealized geometries. The details for crystallographic data and relevant structure refinement are listed in Tables S1 and S2.†

Density functional theory (DFT) calculations

The Vienna *Ab initio* Simulation Package (VASP) with projector augmented wave (PAW) potentials was used for the first principles calculations.[54,55] The Perdew–Burke–Ernzerhof (PBE) functional of the generalized gradient approximation (GGA) was adopted as the exchange correlation function.[56] The threshold of 10^{-4} eV and the plane-wave cutoff energy of 400 eV were set for the self-consistent-field convergence of the total electronic energy. The adsorption energy (ΔE_{ad}) was calculated as:

$$\Delta E_{ad} = E(\text{fram} + \text{ad}) - E(\text{fram}) - E(\text{ad}) \quad (7)$$

where E(fram + ad) is the energy of the framework with one adsorbed Cs^+ or Sr^{2+} ion, and E(fram), and E(ad) are the energies of the framework and one Cs^+ or Sr^{2+} ion, respectively.

Results and discussion

Synthesis

CdSnSe-1 was prepared by reacting $CdCl_2\cdot 2.5H_2O$, Sn and Se in a deep eutectic solvent (DES) consisting of diethylamine hydrochloride and *N*,*N*′-dimethylurea in a molar ratio of 1 : 2.

According to our previous studies, DESs prove to be excellent media for the preparation of metal chalcogenides owing to their bifunctional role as both a solvent and a source of templates.[48,49,57–61] For example, the DES employed here provides a unique ionic environment that facilitates faster dissolution of reagents and crystal growth of the product, resulting in a relatively shorter reaction time (3 days) and higher yield (70.7%) for **CdSnSe-1**. In addition, *N*,*N*′-dimethylurea underwent *in situ* hydrolysis during the reaction and the generated methylammonium cations were important charge-compensating and structure-directing agents to create appropriate chemical environments for metal adsorption. It is noticeable that $N_2H_4{\cdot}H_2O$ (98%) was added to the reaction system and the $N_2H_4{\cdot}H_2O$: *N*,*N*′-dimethylurea molar ratio needed to be tuned to 2.36 : 1 for isolation of the optimal **CdSnSe-1** product. The decomposition of $N_2H_4{\cdot}H_2O$ gives ammonium species that perform as co-templates with the methylammonium cations. Such a co-templating mechanism integrates well with the broken symmetry of the cluster due to the introduction of a vacant site, which accounts for the formation of voids with distinct chemical environments and adsorption selectivity.

Structural description

CdSnSe-1 crystallizes in the trigonal *R*3*m* space group, featuring an anionic framework of $[Cd_4Sn_3Se_{13}]_n^{6n-}$ templated by mixed methylammonium and ammonium cations. Isomorphic frameworks were also observed in compounds $K_6Cd_4Sn_3Se_{13}$ and $K_3Rb_3Zn_4Sn_3Se_{13}$ where alkaline metal ions were present as counter cations.[62,63] The $[Cd_4Sn_3Se_{16}]^{12-}$-constructing block for the 3D framework appears to be a mono-lacunary derivative from the plenary P1-$[Cd_4Sn_4Se_{17}]^{10-}$ cluster upon removing one $[SnSe]^{2+}$ group at the terminal position (Fig. 2a). Each lacunary $[Cd_4Sn_3Se_{16}]^{12-}$ cluster interconnects with six adjacent ones *via* the apical or impending Se^{2-} ligands (Se(2)) to form an anionic $[Cd_4Sn_3Se_{13}]_n^{6n-}$ open framework (Fig. 2b and c). The framework possesses intersecting micropores, whose trigonal $\{Cd_5Sn_4Se_9\}$ cross-section is large enough (11.82 × 11.15 Å^2) for the transfer of hydrated Cs^+ (r_H = 3.29 Å) and Sr^{2+} (r_H = 4.12 Å) ions (Fig. 2d and Fig. S1†).[64] Equivalent amounts of mixed ammonium and methylammonium were filled in the void spaces as charge-compensating agents. These cations exhibit relatively weak electrostatic interactions and hydrogen bonds with the framework, endowing them with promising mobilities that would undoubtedly facilitate the Cs^+ and Sr^{2+} ion exchange process.

Characterization of the exchange-saturated products

The Cs^+ and Sr^{2+} exchange-saturated products, *i.e.* $Cs_{5.6}[CH_3NH_3]_{0.2}[NH_4]_{0.2}Cd_4Sn_3Se_{13}{\cdot}3.5H_2O$ (**CdSnSe-1Cs**) and $Sr_{2.85}[CH_3NH_3]_{0.15}[NH_4]_{0.15}Cd_4Sn_3Se_{13}{\cdot}6.5H_2O$ (**CdSnSe-1Sr**), keep the block-like crystal morphology very like that of the **CdSnSe-1** exchanger, apart from the color change from orange to red and the fracture-caused rough surfaces (Fig. 3a). As shown in Fig. 3b, the compounds are shown to be direct semiconductors as the photon energy ($h\nu$) and the band-gap energy (E_g) have a simple relation as $\alpha h\nu$ = const. × $(h\nu - E_g)^{1/2}$, where α can be computed using the Kubelka–Munk function $\alpha/S = F(R) = (1-R)^2/2R$.[52] It is clear that the ion exchange leads to a red shift of optical band gaps from 2.14 eV (**CdSnSe-1**) to 1.66 eV (**CdSnSe-1Cs**) or 1.64 eV (**CdSnSe-1Sr**), in consistent with the color change of appearance. EDS analysis and element mapping images illustrate that Cs^+ and Sr^{2+} ions enter the exchanger and exhibit a homogeneous distribution in the exchanged samples (Fig. 3c and Fig. S2–S4†). Elemental analysis suggests a significant decrease in N components in the solid product upon the Cs^+ and Sr^{2+} uptake, reconfirming the ion exchange mechanism for the adsorption process. All the pristine and exchanged materials were characterized by powder XRD (Fig. 3d). They

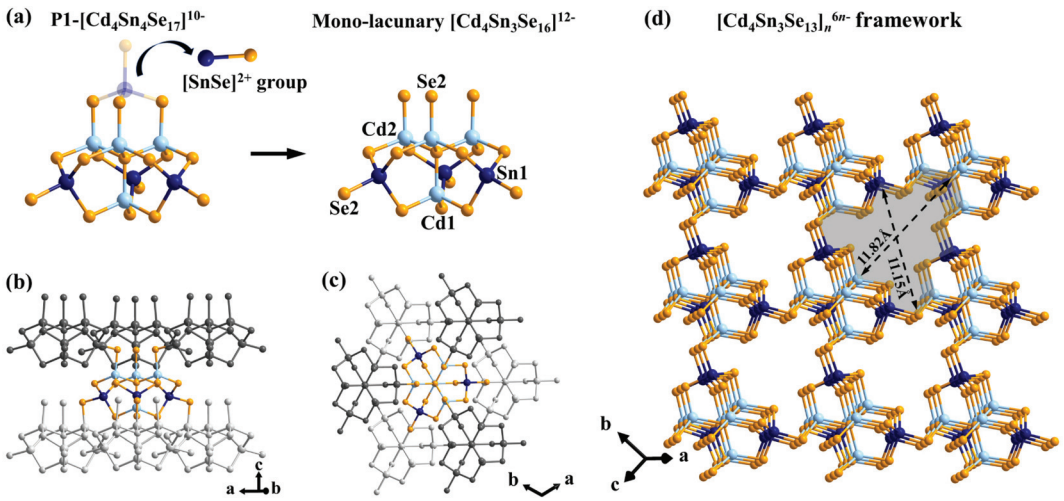

Fig. 2 (a) Structural derivation from a plenary P1-$[Cd_4Sn_4Se_{17}]^{10-}$ cluster to a mono-lacunary $[Cd_4Sn_3Se_{16}]^{12-}$ cluster. (b and c) Side and top view of the interconnection between the central $[Cd_4Sn_3Se_{16}]^{12-}$ cluster (shown in color) and six surrounding ones (shown in pale and dark gray) in **CdSnSe-1**. (d) Representation of the $[Cd_4Sn_3Se_{13}]_n^{6n-}$ framework of **CdSnSe-1**. The gray-highlighted moiety is the $\{Cd_5Sn_4Se_9\}$ window.

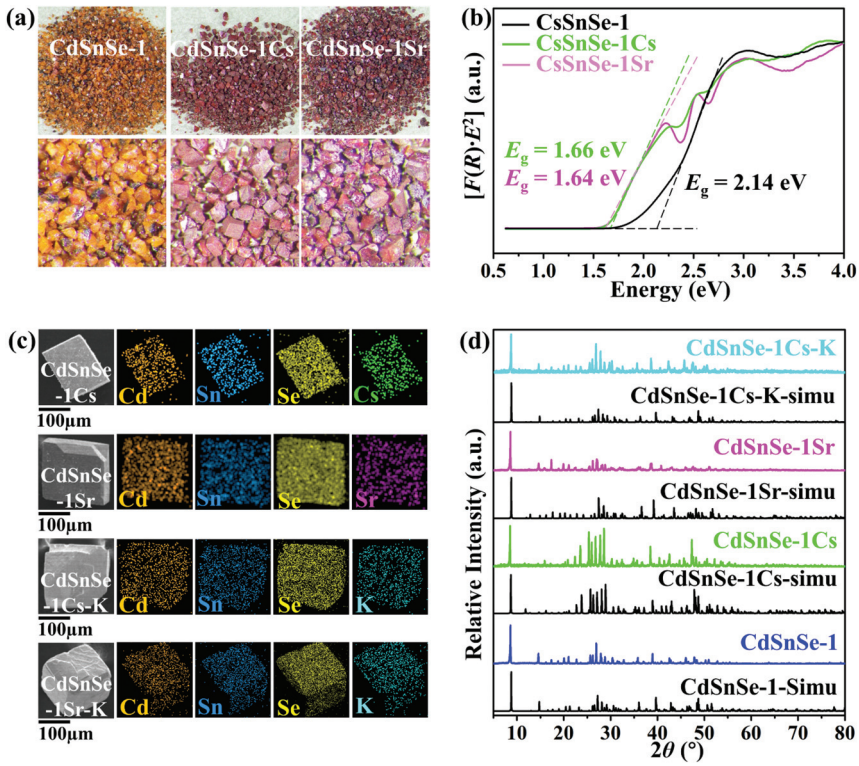

Fig. 3 (a) Exterior appearances, (b) Kubelka–Munk spectra, (c) SEM and elemental mapping images and (d) powder XRD patterns of pristine **CdSnSe-1** and ion-exchanged products **CdSnSe-1Cs** and **CdSnSe-1Sr**. Eluted products **CdSnSe-1Cs-K** and **CdSnSe-1Sr-K** are also included in (c) and (d).

show similarity in diffraction patterns but distinction in 2θ values, peak numbers and intensities, suggesting that the ion exchange is an isotactic process. The retention of the framework is further illustrated by single-crystal structures (as will be discussed below in detail), whose simulated powder XRD patterns match well with the experimental ones. In addition, 200 kGy β or 100 kGy γ radiation would not cause structural and crystal damage to **CdSnSe-1** (Fig. S5†), illustrating the good radiolytic stability of the exchanger for capturing radioactive isotopes.

High-resolution XPS of **CdSnSe-1**, **CdSnSe-1Cs** and **CdSnSe-1Sr** show characteristic peaks for Cd and Sn elements (Fig. 4a). The binding energies of 495.3 (Sn $3d_{3/2}$) and 486.9 eV (Sn $3d_{5/2}$) demonstrate the +IV oxidation state for Sn during the ion exchange process, without any chemical reduction being detected. The characteristic peaks for the adsorbed Cs^+, Sr^{2+} and K^+ ions are assigned to binding energies of 738.1 (Cs $3d_{3/2}$), 724.2 (Cs $3d_{5/2}$), 135.9 (Sr $3d_{3/2}$), 133.8 (Sr $3d_{5/2}$), 295.5 (K $2p_1$) and 293.0 eV (K $2p_3$) (Fig. 4b). Notably, the binding energy for Se $3d_{3/2}$ (54.3 eV) is raised to higher values upon ion exchange (54.6 eV for Cs^+ adsorption, 54.7 eV for Sr^{2+} adsorption and elution by K^+), which implies a decrease in the negative charge density of Se^{2-} owing to the electron transfer to Cs^+, Sr^{2+} and K^+ ions (Fig. 4c). This implies that the adsorbed metal ions interact more intensely with the Se^{2-} ions compared with the original ammonium and methylammonium ions. All these characteristic peaks are presented in the survey spectra (Fig. 4d).

Ion exchange kinetics and isotherms

The uptake of Cs^+ and Sr^{2+} ions by **CdSnSe-1** single crystals with increasing contact time was investigated (Fig. 5a and b). The removal rates of Cs^+ and Sr^{2+} were 71.06% and 74.45% within 4 h and remained almost unchanged after 24 h. At equilibrium (48 h for example), the removal rate of Sr^{2+} (94.85%) was slightly higher than that of Cs^+ (91.72%), implying an intrinsically stronger affinity of **CdSnSe-1** to Sr^{2+}. The plots of t/q_t *vs.* t were well fitted with the pseudo-second-order model, giving high correlation coefficients R^2 of 0.99982 for Cs^+ and 0.99922 for Sr^{2+} (insets of Fig. 5a and b). The adsorption rate constants k_2 of **CdSnSe-1** were determined to be 0.00212 g mg^{-1} min^{-1} for Cs^+ and 0.00373 g mg^{-1} min^{-1} for Sr^{2+}, which are comparable with the values for some other metal selenides, *e.g.*, CuGeSe-1 (0.00635 g mg^{-1} min^{-1} for Cs^+)[48] and AgSnSe-1 (0.00895 g mg^{-1} min^{-1} for Cs^+).[49] The calculated values of q_e were 5.79 mg g^{-1} for Cs^+ and 5.85 mg g^{-1} for Sr^{2+}, in line with the practical ones (5.61 mg g^{-1} for Cs^+ and 5.75 mg g^{-1} for Sr^{2+}). These reconfirm the superior fit of the pseudo-second-order kinetic model to experimental data, suggesting that the chemical adsorption is the rate-determining step in the Cs^+ or Sr^{2+} adsorption process.

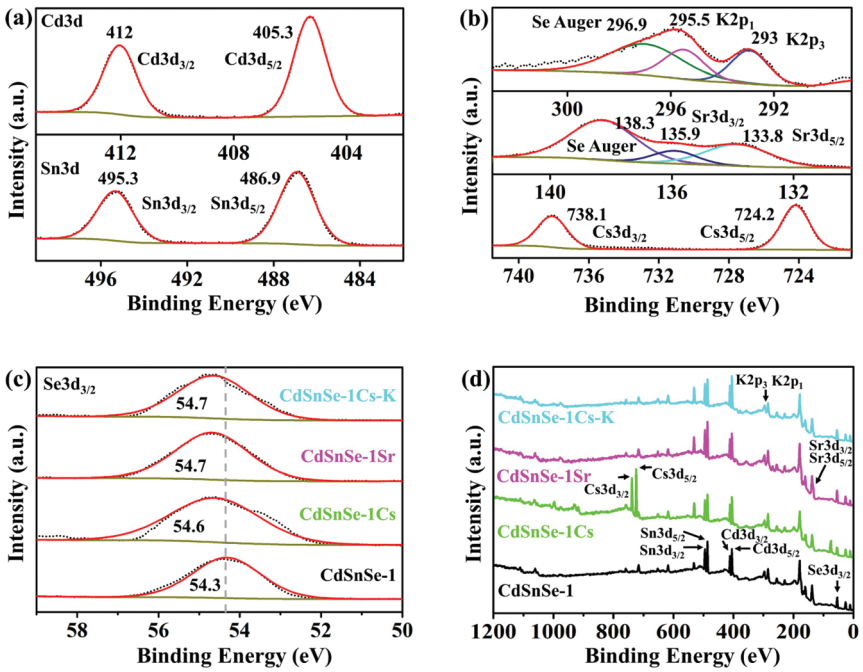

Fig. 4 High-resolution XPS spectra of (a) Cd 3d, Sn 3d, (b) Cs 3d, Sr 3d, K 2p, (c) Se 3d and (d) survey XPS spectra before and after ion exchange with Cs^+, Sr^{2+}, and eluted by K^+. The overall fitting and experimental curves are shown in red solid and black dotted lines, respectively.

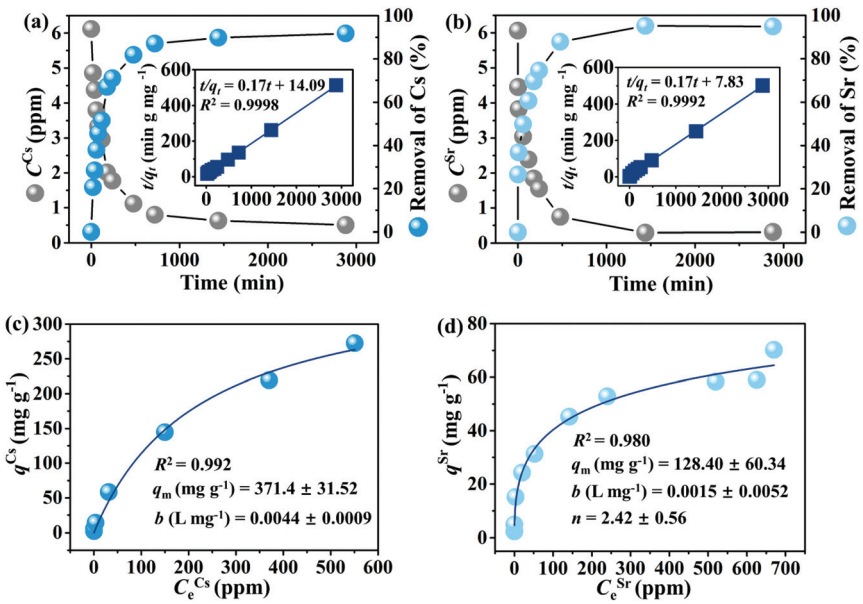

Fig. 5 (a and b) Variation of Cs^+ and Sr^{2+} concentration and their removal rates with contact time t (min). Insert: plot of t/q_t (min g mg^{-1}) *vs.* t according to the kinetic data ($C_0 \sim 6$ ppm, pH = 6, V/m = 1000 mL g^{-1}, room temperature). (c and d) Equilibrium curves of Cs^+ and Sr^{2+} adsorption by **CdSnSe-1** ($C_0^{Cs} \sim 3$–824 ppm, $C_0^{Sr} \sim 3$–741 ppm).

The ion exchange isotherms of **CdSnSe-1** were recorded for Cs^+ ($C_0 \sim 3$–824 ppm) and Sr^{2+} ($C_0 \sim 3$–741 ppm) at room temperature. Fig. 5c and d shows that the exchange capacity of Cs^+ or Sr^{2+} increases with the equilibrium concentration. The equilibrium curve of Cs^+ ion exchange can be fitted well by the Langmuir model ($R^2 = 0.992$), giving a maximum exchange capacity q_m^{Cs} of 371.4 mg g^{-1} that accounts for 94.9% of the theoretical capacity (391.5 mg g^{-1}) (Fig. 5c). The q_m^{Cs} is 1.8–8 times higher than the capacities of commonly used natural or artificially prepared Cs^+ adsorbents like clay (46.3 mg g^{-1}),[65] Zeolite A (207.5 mg g^{-1}),[66] titanium silicate TAM-5 (191.8 mg g^{-1}),[67] polyoxometalates I-as (134 mg g^{-1}),[68] and HKUST-1

(153 mg g^{-1}),[69] and is comparable with those of some best metal chalcogenide materials such as KMS-2 (531.7 mg g^{-1}),[36] InSnOS (537.7 mg g^{-1})[46] and FJSM-SnS (408.9 mg g^{-1}) (Tables S7 and 8†).[38] As for Sr^{2+} exchange, the Langmuir–Freundlich isotherm model fits better with the equilibrium curve (R^2 = 0.980) than the Langmuir one (R^2 = 0.939) (Fig. 5d). The higher Langmuir–Freundlich constant (n = 2.42) indicates that the adsorption deviates from the Langmuir isotherm model (n = 1),[37,70] which is reasonable because the number of adsorbed Sr^{2+} ions is only half that of the exchanged ammonium and methylammonium cations and thereby results in a lower surface coverage. The maximum exchange capacity q_m^{Sr} was determined to be 128.4 mg g^{-1}, which is ~99.5% of the theoretical capacity (129.1 mg g^{-1}). A complete ionic substitution is rarely reported for metal chalcogenide Sr^{2+} exchangers, whose cation-accessible space is commonly insufficient for the accommodation of large hydrated Sr^{2+} (*e.g.* $[Sr(H_2O)_6]^{2+}$) ions in a full stoichiometric number.[38,71] In contrast, the q_m^{Sr} of **CdSnSe-1** exceeds those of the oxide adsorbents, *e.g.* clay (39.7 mg g^{-1}),[65] $Na_2V_6O_{16}{\cdot}3H_2O$ (96.4 mg g^{-1}),[72] SZ-4 (117.9 mg g^{-1}),[73] and FJSM-CA (21.3 mg g^{-1}),[74] and even ranks **CdSnSe-1** ahead of some of the best metal chalcogenides like KMS-1 (77 mg g^{-1}),[35] KMS-2 (86.89 mg g^{-1}),[36] KTS-3 (102 mg g^{-1}),[37] NaTS (80 mg g^{-1}),[43] InS-1 (105.35 mg g^{-1}),[40] and ZnSnS-1 (124.2 mg g^{-1}),[39] and very close to FJSM-SnS-4 (141.22 mg g^{-1})[75] and the record-holder InS-2 (143.29 mg g^{-1}).[41]

The excellent Cs^+ and Sr^{2+} exchange capacities stem from the high negative charge density of the $[Cd_4Sn_3Se_{13}]_n^{6n-}$ framework, which was calculated to be 3.27×10^{-3} according to the equation $\rho = z/M_r$.[40] For each building block, the introduction of one vacant site into the plenary P1-$[Cd_4Sn_4Se_{17}]^{10-}$ cluster brings about a reduced molecular weight (from 2266.8 to 2069.1) and increased negative charge number (from −10 to −12), synergistically enhancing the negative charge density of the newly formed lacunary cluster. This pronounced ρ value exceeds those of other selenide ion exchangers like $[NH_4]_4In_{12}Se_{20}$ (1.35×10^{-3}),[76] CuGeSe-1 (1.93×10^{-3})[48] and AgSnSe-1 (1.53×10^{-3}),[49] and it compares well with those of extensively studied metal sulfides such as KMS-1 (1.94 to 3.89 $\times 10^{-3}$),[71] KMS-2 (1.99 to 4.40 $\times 10^{-3}$)[36] and FJSM-SnS (3.44×10^{-3}).[38] Consequently, the rich negative charges of the $[Cd_4Sn_3Se_{13}]_n^{6n-}$ framework need to be compensated by a great quantity of ammonium and methylammonium cations, endowing **CdSnSe-1** with a high theoretical exchange capacity for Cs^+ and Sr^{2+}.

Elution

The elution of Cs^+ and Sr^{2+} ions can be easily achieved by exposing Cs^+- and Sr^{2+}-laden products to highly concentrated K^+ (1 M KCl). EDS analysis and elemental mapping indicate that 100% of Cs^+ and 88.3% of Sr^{2+} were replaced by K^+ (Fig. 3c and Fig. S10, S11†), giving the analogous potassium salts of cadmium selenidostannate, *i.e.* $K_6Cd_4Sn_3Se_{13}{\cdot}5H_2O$ (**CdSnSe-1Cs-K**) and $K_{5.3}Sr_{0.35}Cd_4Sn_3Se_{13}{\cdot}6.5H_2O$ (**CdSnSe-1Sr-K**). Once eluted, the original block-like morphology of the exchanger was well retained, with no obvious cracks or fractures. The powder XRD patterns shown in Fig. S12† indicate the retention of the framework upon elution treatment, reflecting an excellent mechanical resistance for the alternating transfer of cations. Moreover, the eluted products can be further used for adsorption towards Cs^+ and Sr^{2+} (Fig. S13 and S14†), whose removal rates were 64.97% and 61.54% within 4 h and remained almost unchanged after 24 h. The equilibrium removal rates of Cs^+ and Sr^{2+} were determined to be 92.64% and 98.01%, comparable with those of the pristine exchanger. The retention of the framework structure and exchange performance reveals a recycling potential of the material for industry practice.

Structural and theoretical investigation of the ion exchange

Accurate structural investigations on the Cs^+ and Sr^{2+} exchange-saturated and eluted products were performed by means of single-crystal XRD to give illuminating insights into the ion exchange mechanism. All four samples, *i.e.* **CdSnSe-1Cs**, **CdSnSe-1Sr**, **CdSnSe-1Cs-K** and **CdSnSe-1Sr-K**, crystallize in the same trigonal *R3m* space group as that of **CdSnSe-1**, featuring the same parent framework architecture. Upon the uptake of Cs^+, the unit cell volume expands by 2.5%, from 3097.30(6) to 3176.24(11) $Å^3$, as the length of c axis is increased from 16.0233(2) to 16.4222(4) Å. This stems probably from the steric interactions from larger Cs^+ ions to the framework, which is mirrored by an enlargement of the Cd(2)–Se(2)–Sn(1) bond angle from 97.35 to 99.23°, as well as a broadening of the $\{Cd_5Sn_4Se_9\}$ window from 11.82 × 11.15 to 12.01 × 11.15 $Å^2$. Once the Cs^+ (structural ionic radius r_s: 1.69 Å) is eluted by the smaller K^+ (r_s:1.33 Å),[64] the a/b and c axes are shortened to 14.8258(2) and 16.0744(4) Å, respectively, resulting in a unit cell contraction back to 3059.86 (11) $Å^3$ that is 1.2% smaller even than that of the pristine exchanger. In comparison, although the growth of the c axis was also observed for the incorporation of Sr^{2+}, the a and b axes were contrarily shortened from 14.94000(10) to 14.7181(2) Å due to the fact that the (alkyl)ammonium ions were replaced by Sr^{2+} in a half quantity owing to the +2 charge on the latter being twice as high as that on the former. This contributes to an overall retention of the unit cell volume upon Sr^{2+} exchange. The framework flexibility of materials bears importance for some specific functions such as separation, purification, and molecular/ion recognition.[77–80] Nevertheless, the dynamic response has rarely been investigated for metal selenide exchangers, being limited to examples like $K_{14-x}H_xCd_{15}Sn_{12}Se_{46}$ ($x \approx 7$),[47] $[NH_4]_4In_{12}Se_{20}$,[76] CuGeSe-1,[48] and AgSnSe-1,[49] hampering the deeper understanding of the selective adsorption mechanism.

The introduction of a vacant site reduces the cluster symmetry from T_d to C_{3v}, with a 3-fold rotation axis passing through the vacant site and the center of three apical vertices of the cluster. This configuration gives rise to an obvious distinction in chemical environment between the space voids that are positioned around the vacant site (void I) of the cluster and that at the hollow between two apical vertices (void II), respectively (Fig. 6a and b). Void I is occupied by one methyl-

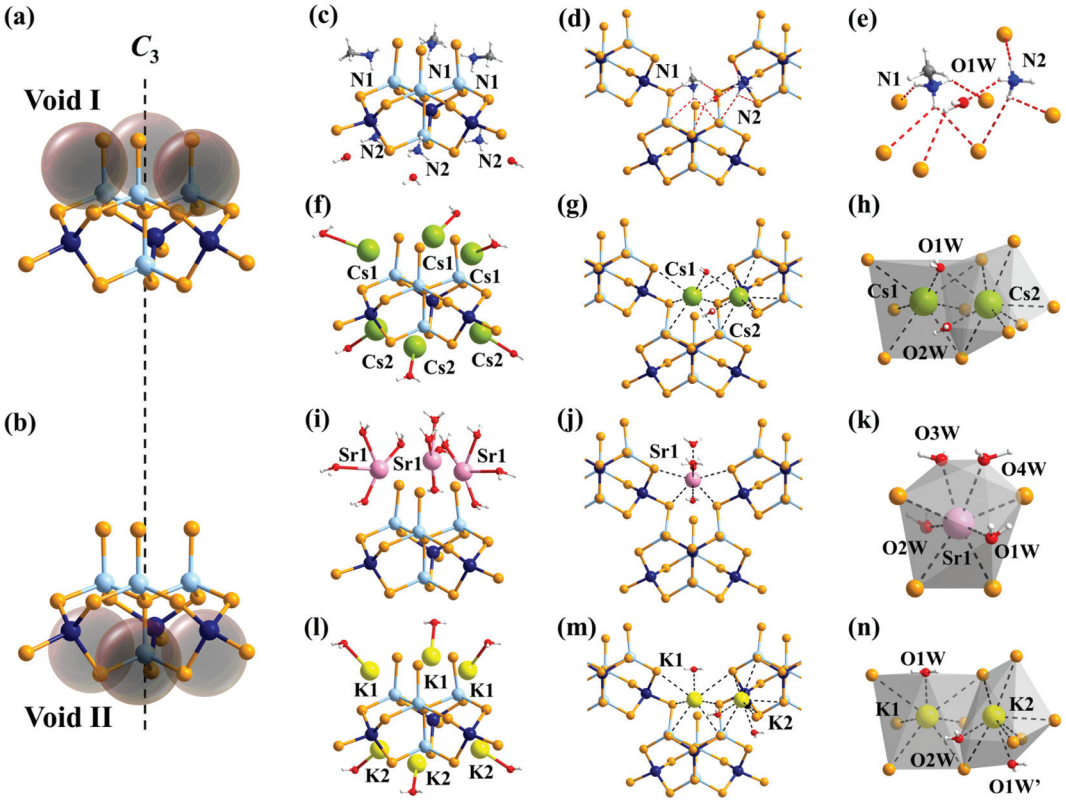

Fig. 6 (a and b) Representations of voids I and II around the mono-lacunary $[Cd_4Sn_3Se_{16}]^{12-}$ cluster. Positions and coordination environments of ammonium/methylammonium, Cs^+, Sr^{2+} and K^+ in (c–e) **CdSnSe-1**, (f––h) **CdSnSe-1Cs**, (i–k) **CdSnSe-1Sr** and (l–n) **CdSnSe-1Cs-K/CdSnSe-1Sr-K**.

ammonium cation with the methyl group pointing outwards from the cluster, while void II is filled by an inner ammonium cation together with an outer water molecule. Consequently, for each cluster, there are three methylammonium cations evenly distributed around the truncated vertex, and three extra ammonium cations located at the edge centers of the bottom plane generated by the other three vertices (Fig. 6c–e). According to the elemental analysis, 93.3% of the ammonium and methylammonium ions are substituted by Cs^+ ions, which are located at both voids I (Cs(1)) and II (Cs(2)) with equivalent occupancies (Fig. 6f). Both $Cs(1)^+$ and $Cs(2)^+$ are surrounded by six Se^{2-} ions and the Cs···Se distance ranges from 3.6270 (15) to 3.9320(17) Å. A bridging aqua ligand (O(1W), ~50% occupancy) is located between adjacent $Cs(1)^+$ and $Cs(2)^+$ ions, and there is another extra water molecule (O(2W), ~50% occupancy) detected close to $Cs(2)^+$ (Fig. 6g and h). The case becomes different for the Sr^{2+}-laden product, where more than 95% (based on elemental analysis) ammonium and methylammonium ions are replaced. Distinct from the two-positional distribution of Cs^+, all the Sr^{2+} ions are located at a new site (denoted as void III) that remains in parallel with the plane generated by two impending $Se(2)^{2-}$ ions around the vacant site and two bridging $Se(4)^{2-}$ ions from two adjacent clusters (Fig. 6i). In this case, each Sr^{2+} interacts with the overall four Se^{2-} ions of the framework, featuring a shorter Sr···Se distance range of 3.212(4)–3.275(3) Å compared with Cs···Se interaction. The remaining space of the Sr^{2+} coordination sphere is filled with approximately two aqua ligands that are distributed at four positions (O(1W), O(2W), O(3W) and O(4W)), forming a $\{(H_2O)_2Sr\}$ plane that is perpendicular to the $\{Se_4Sr\}$ plane (Fig. 6j and k). The higher hydration degree of the adsorbed Sr^{2+} ($Sr^{2+}:H_2O \approx 1:2$ in molar ratio) compared with Cs^+ ($Cs^+:H_2O \approx 2:1$ in molar ratio) is in good agreement with the hydrated radius order of r_H^{Sr} (4.12 Å) > r_H^{Cs} (3.29 Å) in aqueous solution. Upon elution, both Cs^+ and Sr^{2+} adsorbed in the exchanger would be substituted by K^+ ions, which occupy almost the same positions as the Cs^+ because of their common alkaline metal nature (Fig. 6l). The hydration degree of the K^+ salt analog is detected to be higher than the Cs^+-laden product, in accordance with the similarity of Cs^+ and K^+ in hydrated radii (Cs^+, 3.29 Å; K^+, 3.31 Å), but distinction in structural radii (Cs^+, 1.69 Å; K^+, 1.33 Å) (Fig. 6m and n). That is to say, the hydration tendency of $Sr^{2+} > K^+ > Cs^+$ is well kept in the crystal lattice, where the Sr^{2+}, K^+ and Cs^+ metal centers are coupled with approximately two, one and one-half water molecules, respectively.

Density functional theory (DFT) calculations were further conducted on the crystal structures of exchanged products to explore the efficiency of voids for Cs^+ and Sr^{2+} capture (Fig. 7 and Table S9†). The adsorption energy of each Cs^+ at voids I and II was calculated to be −51.95 and −51.79 kcal mol^{-1}, respectively, which indicates a favorable thermodynamic

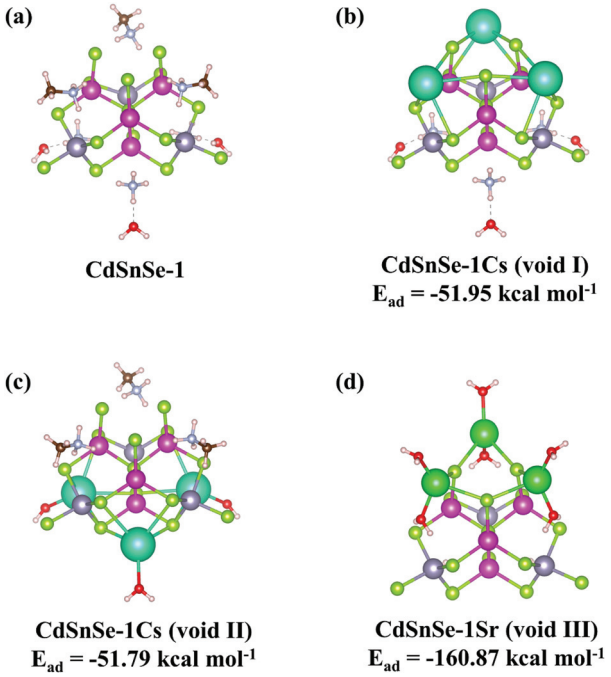

Fig. 7 DFT-modified structures of (a) **CdSnSe-1**, (b) **CdSnSe-1Cs** (void I), (c) **CdSnSe-1Cs** (void II) and (d) **CdSnSe-1Sr** (void III) showing the position of ammonium/methylammonium, Cs^+ and Sr^{2+} related to the mono-lacunary cluster and the corresponding coordination environments. Extra Cs···Se and Sr···Se interactions with adjacent clusters are not shown for clarity.

process for the capture of Cs^+ by both two nonequivalent sites (Fig. 7b and c). This agrees well with the almost complete substitution of ammonium or methylammonium by Cs^+ and the equivalent distribution in quantity over these two sites that is revealed by elemental analysis, TG curves (Fig. S15†) and single-crystal refinement. In comparison, the adsorption energy of Sr^{2+} at void III was determined to be −160.87 kcal mol^{-1} (Fig. 7d), which is even higher than the values recorded for Cs^+ adsorption. This reveals a stronger affinity of the **CdSnSe-1** framework to Sr^{2+} than Cs^+, which certificates the conclusion drawn from the aforementioned exchange kinetic study. It is further reflected by the absence of Cs^+ but the small amount of residual Sr^{2+} in the exchanger upon elution with concentrated K^+. Calculations were also conducted on the hypothetical adsorption of Sr^{2+} in void I or II, but the results cannot converge reasonably, or instead give the fragmentation of the molecules. This suggests the invalidity of original sites occupied by ammonium or methylammonium for the capture of Sr^{2+}, which is probably caused by the stereochemical constraints of the larger hydrated Sr^{2+} compared with Cs^+ and/or the unbalanced charge distribution over a crystal lattice that is not beneficial for stabilization. In one word, the exiting "visualization" of the complete Cs^+ and Sr^{2+} adsorption and K^+-elution processes through well-refined single-crystal structures not only underlines the robust and flexible framework of the **CdSnSe-1** exchanger, but also supplies important information for the recognition of ionic species varying in size, charge and other physicochemical properties.

Effects of pH on the ion exchange

Because the radioactive Cs^+- and Sr^{2+}-contaminated water would be acidic or alkaline, it is highly desirable to investigate the influence of solution pH on the performance of **CdSnSe-1**. The ion exchange features a bimodal-shape variation of K_d with pH, where the peak values are positioned at pH 5 (1.11×10^4 mL g^{-1}) and 11 (1.42×10^4 mL g^{-1}) for Cs^+, and pH 6 (1.96×10^4 mL g^{-1}) and 11 (1.50×10^4 mL g^{-1}) for Sr^{2+} (Fig. 8a and b). In general, a K_d larger than 10^4 mL g^{-1} is evaluated as good for adsorbents, and **CdSnSe-1** compares well with some outstanding bi-functional Cs^+ and Sr^{2+} exchangers with K_d values ranging from 10^3 to 10^5 mL g^{-1}, such as KMS-1 (K_d^{Cs} = 2×10^4 mL g^{-1}; K_d^{Sr} = 1.52×10^5 mL g^{-1}),[35,71] KMS-2 (K_d^{Cs} = 4.56×10^3 mL g^{-1}; K_d^{Sr} = 1.45×10^5 mL g^{-1}),[36] KTS-3 (K_d^{Cs} = 5.5×10^4 mL g^{-1}; K_d^{Sr} = 3.9×10^5 mL g^{-1}),[37] and FJSM-SnS (K_d^{Cs} = 2.36×10^3 mL g^{-1}; K_d^{Sr} = 8.89×10^4 mL g^{-1}).[38] The higher K_d values that occur at weakly acidic and alkaline conditions probably stem from the increase in ionic strength. Actually, both K_d^{Cs} and K_d^{Sr} remain at a level higher than 3.70×10^3 mL g^{-1} over pH 4–12, indicating a remarkable acid/base resistance of exchange performance on **CdSnSe-1**. Especially, **CdSnSe-1** still exhibits superior removal efficiencies for Sr^{2+} at pH 3 (K_d^{Sr} = 1.18×10^3 mL g^{-1}) and pH 13 (K_d^{Sr} = 7.46×10^2 mL g^{-1}), outperforming most metal chalcogenide Sr^{2+} exchangers under highly acidic and alkaline conditions. Powder XRD measurements reveal a good structural stability of **CdSnSe-1** at pH 4–13 for Cs^+ adsorption and pH 3–13 for Sr^{2+} adsorption (Fig. S17†). Stronger acidic (pH 0–2) or alkaline (pH 14) environments result in the collapse of the exchanger framework and give black residues (Fig. S18 and S19†), and thus give rise to worse adsorption performances with R < 35.54% for both ions. In addition, the initial solutions at pH 4–10 were finally neutralized to pH 8.5–10.1 for Cs^+ and pH 7.9–9.4 for Sr^{2+}, suggesting a buffering role of **CdSnSe-1** in accepting or donating protons during the ion exchange processes (Fig. 8a and b).

Effects of coexisting ions on the ion exchange

The waste solution may contain Na^+, K^+, Mg^{2+} and Ca^{2+} ions that would influence the Cs^+, Sr^{2+} exchange. Fig. 8c and d shows the variation of K_d^{Cs} and K_d^{Sr} with the concentration (0.1, 1, 10 and 100 mmol L^{-1}) of each individual coexisting ion. Na^+, Mg^{2+} and Ca^{2+} exhibit a marginal influence on the Cs^+ adsorption, where the K_d^{Cs} values are kept at higher than 10^3 mL g^{-1} even when the concentrations of these ions are increased to 100 mmol L^{-1}. In contrast, the adverse impact of K^+ is more significant, as evidenced by the decrease in K_d^{Cs} to 2.68×10^2 mL g^{-1} in the presence of K^+ (100 mmol L^{-1}). This arises from the comparability of Cs^+ and K^+ in both hydrated (Cs^+, 3.29 Å; K^+, 3.31 Å) and structural ionic radii (Cs^+, 1.69 Å; K^+, 1.33 Å). For Sr^{2+} adsorption, less concentrated (0.1–10 mmol L^{-1}) Na and K^+ ions would not reduce but would raise the K_d^{Sr} up to a level higher than 2.22×10^4 mL g^{-1}. Especially, the K_d^{Sr} can even reach 9.11×10^4 and 8.17×10^4 mL

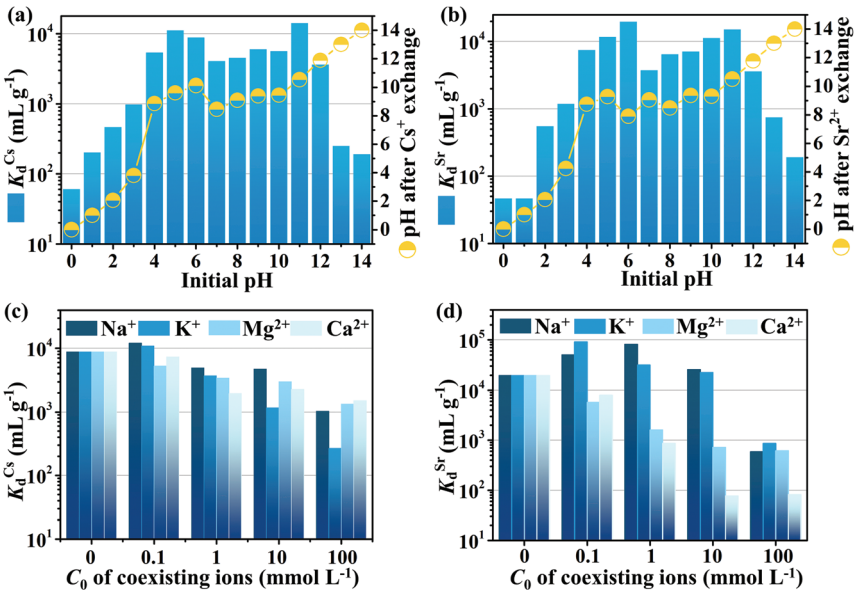

Fig. 8 Variation of K_d with (a and b) solution pH and (c and d) increasing concentrations of coexisting ions (pH ~6) for Cs^+ and Sr^{2+} ion exchange by **CdSnSe-1**. The end pH values after exchange are shown as yellow scatters in (a) and (b). Note: C_0 ~ 6 ppm, 25 °C, V/m = 1000 mL g^{-1}, contact time = 24 h.

g^{-1} in the presence of 0.1 mmol L^{-1} K^+ and 1 mmol L^{-1} Na^+, respectively. This may be ascribed to the increase in overall ionic strength that is analogous to the observation in the pH effect study. Another possible reason is the charge distinction as Sr^{2+} is a divalent cation while Na^+ and K^+ are monovalent cations. In comparison, the uptake of Sr^{2+} is more sensitively affected by Mg^{2+} and Ca^{2+} ions, whose hydrated ionic radii (Mg^{2+}, 4.28 Å; Ca^{2+}, 4.12 Å) are closer to that of Sr^{2+} (4.12 Å) than those of Na^+ (3.58 Å) and K^+ (3.31 Å). The K_d^{Sr} decreases from 1.96 × 10^4 (blank) to 7.18 × 10^2 mL g^{-1} as the concentration of Mg^{2+} is increased to 10 mmol L^{-1}, and if the Mg^{2+} is replaced by Ca^{2+}, the K_d^{Sr} value will decline more sharply to 76.53 mL g^{-1}. The more severe effect of Ca^{2+} than Mg^{2+} can be ascribed to its higher similarity to Sr^{2+} in both structural ionic radius (Mg^{2+}, 0.65 Å; Ca^{2+}, 0.99 Å; Sr^{2+}, 1.13 Å) and chemical properties.

Ion exchange in actual water environments

The Cs^+ and Sr^{2+} (C_0 ~ 6 ppm for each) ion exchange performances of **CdSnSe-1** were also explored in mineral water (MW), tap water (TW) and lake water (LW). The experiments performed in deionized water (DW) were adopted as a control (Fig. 9 and Table S14†). **CdSnSe-1** displays superior Cs^+ adsorption in MW and TW, with corresponding K_d values of 3.43 × 10^3 mL g^{-1} (R = 77.41%) and 3.83 × 10^3 mL g^{-1} (R = 79.31%), respectively. Even in LW, the K_d value is still kept higher than 1.20 × 10^3 mL g^{-1} (R = 54.62%), which can be ascribed to the good resistance of **CdSnSe-1** to relatively highly concentrated Na^+ (683.05 ppm), Mg^{2+} (102.80 ppm) and Ca^{2+} (81.20 ppm). In comparison, the Sr^{2+} exchange is influenced more significantly by the actual environment. Based on the analysis of water quality, the Ca^{2+} concentration follows the order of MW (9.88 ppm) < TW (36.3 ppm) < LW (81.20 ppm). 47.81% and 38.83% of Sr^{2+} can be eliminated from MW and TW, and the removal further drops to 17.05% in LW. This contributes to lower K_d values of 9.16 × 10^2 (MW), 6.35 × 10^2 (TW) and 2.06 × 10^2 mL g^{-1} (LW) compared with those for Cs^+ adsorption.

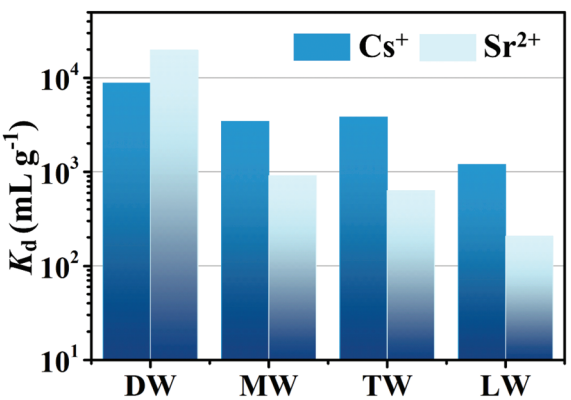

Fig. 9 K_d for Cs^+ and Sr^{2+} ion exchange by **CdSnSe-1** performed in DW, MW, TW and LW.

Conclusion

Efficient remediation of Cs^+ and Sr^{2+} through the ion exchange method was achieved using a cadmium selenidostannate **CdSnSe-1**, whose unique open framework constructed from mono-lacunary supertetrahedral clusters facilitates the systematic investigation of capture and elution mechanism at the molecular level. **CdSnSe-1** exhibits rapid ion exchange kinetics,

wide pH durability, high exchange selectivity and β and γ radiation resistance. Particularly, the $[Cd_4Sn_3Se_{13}]_n^{6n-}$ framework features a large negative charge density of 3.27×10^{-3} that accounts for the superhigh exchange capacities of 371.4 mg g^{-1} for Cs^+ and 128.4 mg g^{-1} for Sr^{2+}. Moreover, the facile elution of adsorbed Cs^+ and Sr^{2+} ions by K^+ endows this material with a promising potential for recycling. Single-crystal structural analysis on the solid at different stages in the "pristine–exchange–elution" cycle supplies instructive information to clarify the uptake and recycle mechanism for Cs^+ and Sr^{2+}. The co-templating effects of mixed methylammonium/ammonium and the broken symmetry of the cluster caused by the vacant site contribute to the formation of two types of voids (I and II) that show adsorption activity for both monovalent Cs^+ and K^+ ions. In comparison, the divalent Sr^{2+} ions with a higher hydration degree exchange with the (alkyl) ammonium cations in a 1 : 2 molar ratio, resulting in their location at a new void (III) closer to the framework and thus higher binding strength. DFT calculations performed on the well-refined crystal structures illustrate the efficiency of **CdSnSe-1** for Cs^+ and Sr^{2+} capture according to the energy variation during the adsorption process. In one word, the "visualized" mechanism research presented here sheds light on a deeper understanding of the structure–function relationship for materials, which is of great significance for methodological innovation in radionuclide remediation.

Conflicts of interest

There are no conflicts to declare.

Acknowledgements

This work was financially supported by the National Natural Science Foundation of China (21701123), the Foundation Enhancement Program (2021-JCJQ-JJ-1061), the Fund of the State Key Laboratory of Structural Chemistry (20190009), and the Fund of the National Engineering Research Center for Optoelectronic Crystalline Materials (OCM-2020-02).

Notes and references

1 M. Aoyagi, The impact of the Fukushima accident on nuclear power policy in Japan, *Nat. Energy*, 2021, **6**, 326–328.
2 T. Ohba, K. Tanigawa and L. Liutsko, Evacuation after a nuclear accident: Critical reviews of past nuclear accidents and proposal for future planning, *Environ. Int.*, 2021, **148**, 106379.
3 P. C. Burns, R. C. Ewing and A. Navrotsky, Nuclear fuel in a reactor accident, *Science*, 2012, **335**, 1184–1188.
4 H. Tazoe, T. Yamagata, K. Tsujita, H. Nagai, H. Obata, D. Tsumune, J. Kanda and M. Yamada, Observation of dispersion in the Japanese coastal area of released ^{90}Sr, ^{134}Cs, and ^{137}Cs from the Fukushima Daiichi nuclear power plant to the sea in 2013, *Int. J. Environ. Res. Public Health*, 2019, **16**, 4094.
5 A. Konoplev, Y. Wakiyama, T. Wada, C. Udy, V. Kanivets, M. M. Ivanov, M. Komissarov, T. Takase, A. Goto and K. Nanba, Radiocesium distribution and mid-term dynamics in the ponds of the Fukushima Dai-ichi nuclear power plant exclusion zone in 2015–2019, *Chemosphere*, 2021, **265**, 129058.
6 N. Kinoshita, K. Sueki, K. Sasa, J.-I. Kitagawa, S. Ikarashi, T. Nishimura, Y.-S. Wong, Y. Satou, K. Handa, T. Takahashi, M. Sato and T. Yamagata, Assessment of individual radionuclide distributions from the Fukushima nuclear accident covering central-east Japan, *Proc. Natl. Acad. Sci. U. S. A.*, 2011, **108**, 19526–19529.
7 K. Sakuma, K. Yoshimura and T. Nakanishi, Leaching characteristics of ^{137}Cs for forest floor affected by the Fukushima nuclear accident: A litterbag experiment, *Chemosphere*, 2021, **264**, 128480.
8 W. Men, F. Wang, W. Yu, J. He, F. Lin, F. Deng, T. Yu, H. Ma and Z. Zeng, Radioactive impacts of the Fukushima Dai-ichi nuclear power plant accident on blue sharks in the Northwest Pacific, *Chemosphere*, 2021, **285**, 131537.
9 D. Alby, C. Charnay, M. Heran, B. Prelot and J. Zajac, Recent developments in nanostructured inorganic materials for sorption of cesium and strontium: Synthesis and shaping, sorption capacity, mechanisms, and selectivity – A review, *J. Hazard. Mater.*, 2018, **344**, 511–530.
10 B. Ding, Z. Wang, X. Wang, W. Yang, S. Wang, C. Li, H. Dai and S. Tao, Sr^{2+} adsorbents produced by microfluidics, *Colloids Surf., A*, 2021, **613**, 126072.
11 M. Castrillejo, N. Casacuberta, C. F. Breier, S. M. Pike, P. Masqué and K. O. Buesseler, Reassessment of ^{90}Sr, ^{137}Cs, and ^{134}Cs in the coast off Japan derived from the Fukushima Dai-ichi nuclear accident, *Environ. Sci. Technol.*, 2016, **50**, 173–180.
12 X.-Y. Zhou, D. A. Sun, Y. Tan and A. Zhou, Canister spacing in high-level radioactive nuclear waste repository, *Ann. Nucl. Energy*, 2020, **141**, 107335.
13 O. Artun, A study of nuclear structure for ^{244}Cm, ^{241}Am, ^{238}Pu, ^{210}Po, ^{147}Pm, ^{137}Cs, ^{90}Sr and ^{63}Ni nuclei used in nuclear battery, *Mod. Phys. Lett. A*, 2017, **32**, 1750117.
14 H. Yoshikawa, S. Sunada, H. Hirakawa, A. Fujimori, S. Elmegerhi, D. Leary and T. A. Kato, Radiobiological characterization of canine malignant melanoma cell lines with different types of ionizing radiation and efficacy evaluation with cytotoxic agents, *Int. J. Mol. Sci.*, 2019, **20**, 841.
15 M. Huang, R. G. Hill and S. C. F. Rawlinson, Strontium (Sr) elicits odontogenic differentiation of human dental pulp stem cells (hDPSCs): A therapeutic role for Sr in dentine repair?, *Acta Biomater.*, 2016, **38**, 201–211.
16 S.-M. Kim, I.-H. Yoon, I. Kim, J.-H. Kim and S.-J. Park, Hydrothermal desorption of Cs with oxalic acid from hydrobiotite and wastewater treatment by chemical precipitation, *Energies*, 2020, **13**, 3284.

17 D. Fang, Y. Wang, H. Liu, H. Zhang, X. Ye, Q. Li, J. Li and Z. Wu, Efficient extraction of Rb^+ and Cs^+ by a precipitation flotation process with ammonium phosphowolframate as precipitant, *Colloids Surf., A*, 2021, **608**, 125581.
18 P. Vaňura, P. Selucký and Z. Asfari, Towards selective separations of monovalent cations by solvent extraction of their calix[4]crown complexes in water–nitrobenzene systems, *J. Mol. Liq.*, 2021, **336**, 116357.
19 K. Patra, B. Sadhu, A. Sengupta, C. B. Patil, R. K. Mishra and C. P. Kaushik, Achieving highly efficient and selective cesium extraction using 1,3-di-octyloxycalix[4]arene-crown-6 in n-octanol based solvent system: experimental and DFT investigation, *RSC Adv.*, 2021, **11**, 21323–21331.
20 F. Ma, Z. Li, H. Zhao, Y. Geng, W. Zhou, Q. Li and L. Zhang, Potential application of graphene oxide membranes for removal of Cs(I) and Sr(II) from high level-liquid waste, *Sep. Purif. Technol.*, 2017, **188**, 523–529.
21 R. K. Vishwakarma, P. K. Narayanam, R. Umamaheswari and K. Sundararajan, Surface modified and functionalized graphene oxide membranes for separation of strontium from aqueous solutions, *J. Environ. Manage.*, 2021, **298**, 113443.
22 S. Ghorbanzadeh Mashkani and P. Tajer Mohammad Ghazvini, Biotechnological potential of Azolla filiculoides for biosorption of Cs and Sr: Application of micro-PIXE for measurement of biosorption, *Bioresour. Technol.*, 2009, **100**, 1915–1921.
23 Y. Hu, X. Guo and J. Wang, Biosorption of Sr^{2+} and Cs^+ onto *Undaria pinnatifida*: Isothermal titration calorimetry and molecular dynamics simulation, *J. Mol. Liq.*, 2020, **319**, 114146.
24 Y. Sun, D. Shao, C. Chen, S. Yang and X. Wang, Highly efficient enrichment of radionuclides on graphene oxide-supported polyaniline, *Environ. Sci. Technol.*, 2013, **47**, 9904–9910.
25 K. Jin, B. Lee and J. Park, Metal-organic frameworks as a versatile platform for radionuclide management, *Coord. Chem. Rev.*, 2021, **427**, 213473.
26 C. W. Kim, N. H. Heo and K. Seff, Framework sites preferred by aluminum in zeolite ZSM-5. Structure of a fully dehydrated, fully Cs^+-exchanged ZSM-5 crystal (MFI, Si/Al=24), *J. Phys. Chem. C*, 2011, **115**, 24823–24838.
27 Y. Li, A. O. Simon, C. Jiao, M. Zhang, W. Yan, H. Rao, J. Liu and J. Zhang, Rapid removal of Sr^{2+}, Cs^+ and UO_2^{2+} from solution with surfactant and amino acid modified zeolite Y, *Microporous Mesoporous Mater.*, 2020, **302**, 110244.
28 Y. Kim, Y. K. Kim, J. H. Kim, M.-S. Yim, D. Harbottle and J. W. Lee, Synthesis of functionalized porous montmorillonite via solid-state NaOH treatment for efficient removal of cesium and strontium ions, *Appl. Surf. Sci.*, 2018, **450**, 404–412.
29 A. S. Semenkova, M. V. Evsiunina, P. K. Verma, P. K. Mohapatra, V. G. Petrov, I. F. Seregina, M. A. Bolshov, V. V. Krupskaya, A. Y. Romanchuk and S. N. Kalmykov, Cs^+ sorption onto Kutch clays: Influence of competing ions, *Appl. Clay Sci.*, 2018, **166**, 88–93.
30 N. Döbelin and T. Armbruster, Microporous titanosilicate AM-2: Ion-exchange and thermal stability, *Microporous Mesoporous Mater.*, 2007, **99**, 279–287.
31 D. Ding, K. Li, D. Fang, X. Ye, Y. Hu, X. Tan, H. Liu and Z. Wu, Novel biomass-derived adsorbents grafted sodium titanium silicate with high adsorption capacity for Rb^+ and Cs^+ in the Brine, *ChemistrySelect*, 2019, **4**, 13630–13637.
32 A. J. Cramer and J. M. Cole, Topological analysis of void space in phosphate frameworks: Assessing storage properties for the environmentally important guest molecules and ions: CO_2, H_2O, UO_2, PuO_2, U, Pu, Sr^{2+}, Cs^+, CH_4, and H_2, *ACS Sustainable Chem. Eng.*, 2016, **4**, 4094–4112.
33 A. Ivanets, V. Milyutin, I. Shashkova, N. Kitikova, N. Nekrasova and A. Radkevich, Sorption of stable and radioactive Cs(I), Sr(II), Co(II) ions on Ti–Ca–Mg phosphates, *J. Radioanal. Nucl. Chem.*, 2020, **324**, 1115–1123.
34 A. L. Hames, P. Tkac, A. Paulenova, J. L. Willit and M. A. Williamson, Investigation of molybdate melts as an alternative method of reprocessing used nuclear fuel, *J. Nucl. Mater.*, 2017, **486**, 158–166.
35 M. J. Manos and M. G. Kanatzidis, Highly efficient and rapid Cs^+ uptake by the layered metal sulfide $K_{2x}Mn_xSn_{3-x}S_6$ (KMS-1), *J. Am. Chem. Soc.*, 2009, **131**, 6599–6607.
36 J. L. Mertz, Z. H. Fard, C. D. Malliakas, M. J. Manos and M. G. Kanatzidis, Selective removal of Cs^+, Sr^{2+}, and Ni^{2+} by $K_{2x}Mg_xSn_{3-x}S_6$ (x=0.5–1) (KMS-2) relevant to nuclear waste remediation, *Chem. Mater.*, 2013, **25**, 2116–2127.
37 D. Sarma, C. D. Malliakas, K. S. Subrahmanyam, S. M. Islam and M. G. Kanatzidis, $K_{2x}Sn_{4-x}S_{8-x}$ (x=0.65–1): A new metal sulfide for rapid and selective removal of Cs^+, Sr^{2+} and UO_2^{2+} ions, *Chem. Sci.*, 2016, **7**, 1121–1132.
38 X.-H. Qi, K.-Z. Du, M.-L. Feng, J.-R. Li, C.-F. Du, B. Zhang and X.-Y. Huang, A two-dimensionally microporous thiostannate with superior Cs^+ and Sr^{2+} ion-exchange property, *J. Mater. Chem. A*, 2015, **3**, 5665–5673.
39 K.-Y. Wang, D. Ding, M. Sun, L. Cheng and C. Wang, Effective and rapid adsorption of Sr^{2+} ions by a hydrated pentasodium cluster templated zinc thiostannate, *Inorg. Chem.*, 2019, **58**, 10184–10193.
40 K.-Y. Wang, M. Sun, D. Ding, H.-W. Liu, L. Cheng and C. Wang, Di-lacunary $[In_6S_{15}]^{12-}$ cluster: Building block of a highly negative charged framework for superior Sr^{2+} adsorption capacities, *Chem. Commun.*, 2020, **56**, 3409–3412.
41 M. Sun, K.-Y. Wang, D. Ding, J.-Y. Zhu, Y.-M. Zhao, L. Cheng and C. Wang, Removal of Sr^{2+} ions by a high-capacity indium sulfide exchanger containing permeable layers with large pores, *Inorg. Chem.*, 2020, **59**, 13822–13826.
42 M. Zhang, P. Gu, Z. Zhang, J. Liu, L. Dong and G. Zhang, Effective, rapid and selective adsorption of radioactive Sr^{2+} from aqueous solution by a novel metal sulfide adsorbent, *Chem. Eng. J.*, 2018, **351**, 668–677.
43 Z. Zhang, P. Gu, M. Zhang, S. Yan, L. Dong and G. Zhang, Synthesis of a robust layered metal sulfide for rapid and

effective removal of Sr^{2+} from aqueous solutions, *Chem. Eng. J.*, 2019, **372**, 1205–1215.

44 Y.-M. Zhao, L. Cheng, K.-Y. Wang, X. Hao, J. Wang, J.-Y. Zhu, M. Sun and C. Wang, pH-Controlled switch over coadsorption and separation for mixed Cs^+ and Sr^{2+} by an acid-resistant potassium thioantimonate, *Adv. Funct. Mater.*, 2022, 2112717.

45 X.-M. Zhang, D. Sarma, Y.-Q. Wu, L. Wang, Z.-X. Ning, F.-Q. Zhang and M. G. Kanatzidis, Open-framework oxysulfide based on the supertetrahedral $[In_4Sn_{16}O_{10}S_{34}]^{12-}$ cluster and efficient sequestration of heavy metals, *J. Am. Chem. Soc.*, 2016, **138**, 5543–5546.

46 L. Wang, H. Pei, D. Sarma, X.-M. Zhang, K. MacRenaris, C. D. Malliakas and M. G. Kanatzidis, Highly selective radioactive $^{137}Cs^+$ capture in an open-framework oxysulfide based on supertetrahedral cluster, *Chem. Mater.*, 2019, **31**, 1628–1634.

47 N. Ding and M. G. Kanatzidis, Acid-induced conversions in open-framework semiconductors: From $[Cd_4Sn_3Se_{13}]^{6-}$ to $[Cd_{15}Sn_{12}Se_{46}]^{14-}$, a remarkable disassembly/reassembly process, *Angew. Chem., Int. Ed.*, 2006, **45**, 1397–1401.

48 H.-W. Liu, K.-Y. Wang, D. Ding, M. Sun, L. Cheng and C. Wang, Deep eutectic solvothermal synthesis of an open framework copper selenidogermanate with pH-resistant Cs^+ ion exchange properties, *Chem. Commun.*, 2019, **55**, 13884–13887.

49 D. Ding, L. Cheng, K.-Y. Wang, H.-W. Liu, M. Sun and C. Wang, Efficient Cs^+–Sr^{2+} separation over a microporous silver selenidostannate synthesized in deep eutectic solvent, *Inorg. Chem.*, 2020, **59**, 9638–9647.

50 J.-H. Tang, J.-C. Jin, W.-A. Li, X. Zeng, W. Ma, J.-L. Li, T.-T. Lv, Y.-C. Peng, M.-L. Feng and X.-Y. Huang, Highly selective cesium(I) capture under acidic conditions by a layered sulfide, *Nat. Commun.*, 2022, **13**, 658.

51 Y.-Y. Liao, J.-R. Li, B. Zhang, H.-Y. Sun, W. Ma, J.-C. Jin, M.-L. Feng and X.-Y. Huang, Robust and flexible thioantimonate materials for Cs^+ remediation with distinctive structural transformation: A clear insight into the ion-exchange mechanism, *ACS Appl. Mater. Interfaces*, 2021, **13**, 5275–5283.

52 *Reflectance Spectroscopy*, ed. W. M. Wendlandt and H. G. Hecht, Interscience, New York, 1966.

53 G. M. Sheldrick, A short history of SHELX, *Acta Crystallogr., Sect. A: Found. Crystallogr.*, 2008, **64**, 112–122.

54 G. Kresse and J. Furthmüller, Efficient iterative schemes for ab initio total-energy calculations using a plane-wave basis set, *Phys. Rev. B: Condens. Matter Mater. Phys.*, 1996, **54**, 11169–11186.

55 G. Kresse and D. Joubert, From ultrasoft pseudopotentials to the projector augmented-wave method, *Phys. Rev. B: Condens. Matter Mater. Phys.*, 1999, **59**, 1758–1775.

56 J. P. Perdew, K. Burke and M. Ernzerhof, Generalized gradient approximation made simple, *Phys. Rev. Lett.*, 1996, **77**, 3865–3868.

57 K.-Y. Wang, D. Ding, S. Zhang, Y. Wang, W. Liu, S. Wang, S.-H. Wang, D. Liu and C. Wang, Preparation of thermochromic selenidostannates in deep eutectic solvents, *Chem. Commun.*, 2018, **54**, 4806–4809.

58 K.-Y. Wang, H.-W. Liu, S. Zhang, D. Ding, L. Cheng and C. Wang, Selenidostannates and a silver selenidostannate synthesized in deep eutectic solvents: crystal structures and thermochromic study, *Inorg. Chem.*, 2019, **58**, 2942–2953.

59 K.-Y. Wang, S. Zhang, H.-W. Liu, L. Cheng and C. Wang, Stepwise conversion from GeO_2 to $[MGe_4S_{10}]_n^{3n-}$ (M=Cu, Ag) polymer via isolatable $[Ge_2S_6]^{4-}$ and $[Ge_4S_{10}]^{4-}$ anions by virtue of templating technique, *Inorg. Chem.*, 2019, **58**, 12832–12842.

60 M. Sun, S. Zhang, K.-Y. Wang, J. Wang, L. Cheng, J.-Y. Zhu, Y.-M. Zhao and C. Wang, Mixed solvothermal synthesis of tn cluster-based indium and gallium sulfides using versatile ammonia or amine structure-directing agents, *Inorg. Chem.*, 2021, **60**, 7115–7127.

61 S. Zhang, M. Sun, K.-Y. Wang, L. Cheng, S. Zhang and C. Wang, Conversion of organically directed selenidostannate into porous SnO_2 exhibiting effective electrochemical reduction of CO_2 to C1 products, *ACS Sustainable Chem. Eng.*, 2021, **9**, 2358–2366.

62 N. Ding, D.-Y. Chung and M. G. Kanatzidis, $K_6Cd_4Sn_3Se_{13}$: A polar open-framework compound based on the partially destroyed supertetrahedral $[Cd_4Sn_4Se_{17}]^{10-}$ cluster, *Chem. Commun.*, 2004, 1170–1171.

63 M. Wu, W. Su, N. Jasutkar, X. Huang and J. Li, An open-framework bimetallic chalcogenide structure $K_3Rb_3Zn_4Sn_3Se_{13}$ built on a unique $[Zn_4Sn_3Se_{16}]^{12-}$ cluster: Synthesis, crystal structure, ion exchange and optical properties, *Mater. Res. Bull.*, 2005, **40**, 21–27.

64 E. R. Nightingale, Phenomenological theory of ion solvation. Effective radii of hydrated ions, *J. Phys. Chem.*, 1959, **63**, 1381–1387.

65 A.-A. M. Abdel-Karim, A. A. Zaki, W. Elwan, M. R. El-Naggar and M. M. Gouda, Experimental and modeling investigations of cesium and strontium adsorption onto clay of radioactive waste disposal, *Appl. Clay Sci.*, 2016, **132–133**, 391–401.

66 A. M. El-Kamash, Evaluation of zeolite A for the sorptive removal of Cs^+ and Sr^{2+} ions from aqueous solutions using batch and fixed bed column operations, *J. Hazard. Mater.*, 2008, **151**, 432–445.

67 Z. Zheng, C. V. Philip, R. G. Anthony, J. L. Krumhansl, D. E. Trudell and J. E. Miller, Ion exchange of group I metals by hydrous crystalline silicotitanates, *Ind. Eng. Chem. Res.*, 1996, **35**, 4246–4256.

68 S. Seino, R. Kawahara, Y. Ogasawara, N. Mizuno and S. Uchida, Reduction-induced highly selective uptake of cesium ions by an ionic crystal based on silicododecamolybdate, *Angew. Chem., Int. Ed.*, 2016, **55**, 3987–3991.

69 S. Naeimi and H. Faghihian, Performance of novel adsorbent prepared by magnetic metal-organic framework (MOF) modified by potassium nickel hexacyanoferrate for removal of Cs^+ from aqueous solution, *Sep. Purif. Technol.*, 2017, **175**, 255–265.

70 M. Arshadi, M. J. Amiri and S. Mousavi, Kinetic, equilibrium and thermodynamic investigations of Ni(II), Cd(II),

Cu(II) and Co(II) adsorption on barley straw ash, *Water Resour. Ind.*, 2014, **6**, 1–17.

71 M. J. Manos, N. Ding and M. G. Kanatzidis, Layered metal sulfides: Exceptionally selective agents for radioactive strontium removal, *Proc. Natl. Acad. Sci. U. S. A.*, 2008, **105**, 3696.

72 S. Sarina, A. Bo, D. Liu, H. Liu, D. Yang, C. Zhou, N. Maes, S. Komarneni and H. Zhu, Separate or simultaneous removal of radioactive cations and anions from water by layered sodium vanadate-based sorbents, *Chem. Mater.*, 2014, **26**, 4788–4795.

73 J. Zhang, L. Chen, X. Dai, L. Zhu, C. Xiao, L. Xu, Z. Zhang, E. V. Alekseev, Y. Wang, C. Zhang, H. Zhang, Y. Wang, J. Diwu, Z. Chai and S. Wang, Distinctive two-step intercalation of Sr^{2+} into a coordination polymer with record high ^{90}Sr uptake capabilities, *Chem*, 2019, **5**, 977–994.

74 W. Ma, B. Hu, J.-L. Li, Z.-Z. Zhang, X. Zeng, J. Jin, Z. Li, S.-T. Zheng, M.-L. Feng and X.-Y. Huang, The uptake of hazardous metal ions into a high-nuclearity cluster-based compound with structural transformation and proton conduction, *ACS Appl. Mater. Interfaces*, 2020, **12**, 26222–26231.

75 J. Li, J. Jin, T. Zhang, W. Ma, X. Zeng, H. Sun, M. Cheng, M. Feng and X. Huang, Rapid and selective uptake of Cs^+ and Sr^{2+} ions by a layered thiostannate with acid–base and irradiation resistances, *ACS ES&T Water*, 2021, **1**, 2440–2449.

76 M. J. Manos, C. D. Malliakas and M. G. Kanatzidis, Heavy-metal-ion capture, ion-exchange, and exceptional acid stability of the open-framework chalcogenide $[NH_4]_4In_{12}Se_{20}$, *Chem. – Eur. J.*, 2007, **13**, 51–58.

77 M. J. Manos, K. Chrissafis and M. G. Kanatzidis, Unique pore selectivity for Cs^+ and exceptionally high NH^{4+} exchange capacity of the chalcogenide material $K_6Sn[Zn_4Sn_4S_{17}]$, *J. Am. Chem. Soc.*, 2006, **128**, 8875–8883.

78 K.-Y. Wang, M.-L. Feng, J.-R. Li and X.-Y. Huang, $[NH_3CH_3]_4[In_4SbS_9SH]$: A novel methylamine-directed indium thioantimonate with Rb^+ ion-exchange property, *J. Mater. Chem. A*, 2013, **1**, 1709–1715.

79 N. Ding and M. G. Kanatzidis, Selective incarceration of caesium ions by Venus flytrap action of a flexible framework sulfide, *Nat. Chem.*, 2010, **2**, 187–191.

80 Y.-M. Zhao, M. Sun, L. Cheng, K.-Y. Wang, Y. Liu, J.-Y. Zhu, S. Zhang and C. Wang, Efficient removal of Ba^{2+}, Co^{2+} and Ni^{2+} by an ethylammonium-templated indium sulfide ion exchanger, *J. Hazard. Mater.*, 2022, **425**, 128007.

